 Human Molecular Genetics, 1998, Vol. 7, No. 6 **999–1009**

L1 knockout mice show dilated ventricles, vermis hypoplasia and impaired exploration patterns

Erik Fransen[1,*], Rudi D'Hooge[2], Guy Van Camp[1], Marleen Verhoye[3], Jan Sijbers[4], Edwin Reyniers[1], Philippe Soriano[5], Hiroyuki Kamiguchi[6], Rob Willemsen[7], Sebastiaan K. E. Koekkoek[8], Chris I. De Zeeuw[8], Peter P. De Deyn[2], Annemie Van der Linden[3], Vance Lemmon[6], R. Frank Kooy[1] and Patrick J. Willems[1]

[1]Department of Medical Genetics, [2]Department of Neurochemistry and Behavior, Born-Bunge Foundation, [3]Bio Imaging Laboratory and [4]Department of Physics, University of Antwerp, B-2610 Antwerp, Belgium, [5]Fred Hutchinson Cancer Research Center, Seattle, WA 18104, USA, [6]Department of Neuroscience, Case Western Reserve University, Cleveland, OH 44106, USA', [7]Department of Clinical Genetics and [8]Department of Anatomy, Erasmus University Rotterdam, NL-3000 DR Rotterdam, The Netherlands

Received January 8, 1998; Revised and Accepted March 10, 1998

L1 is a neural cell adhesion molecule mainly involved in axon guidance and neuronal migration during brain development. Mutations in the human L1 gene give rise to a complex clinical picture, with mental retardation, neurologic abnormalities and a variable degree of hydrocephalus. Recently, a transgenic mouse model with a targeted null mutation in the L1 gene was generated. These knockout (KO) mice show hypoplasia of the corticospinal tract. Here we have performed further studies of these KO mice including magnetic resonance imaging of the brain, neuropathological analysis and behavioral testing. The ventricular system was shown to be abnormal with dilatation of the lateral ventricles and the 4th ventricle, and an altered shape of the Sylvius aqueduct. Additionally, the cerebellar vermis of the KO mice is hypoplastic. Their exploratory behavior is characterized by stereotype peripheral circling reminiscent of that of rodents with induced cerebellar lesions.

INTRODUCTION

L1, also referred to as L1CAM, belongs to the immunoglobulin superfamily (IgSF) of cell adhesion molecules (CAMs). During nervous system development, L1 is involved in neuron–neuron adhesion, neuron–Schwann cell interaction, migration of neurons and in axon outgrowth, pathfinding and fasciculation (1,2). During all these processes, L1 provides a means of adhering to various substrates. It serves as a component of a signal transduction system, permitting neurons to detect specific ligands in their environment, and transmits those signals through intracellular second messenger systems. The extracellular part of L1 interacts with a myriad of adhesion molecules, including L1 itself (3), whereas the cytoplasmic domain provides a link between the extracellular signals and the intracellular machinery of the cell. In addition to its role in the development of the nervous system, L1 has also been implicated in learning and memory (4).

Although L1 has been the focus of many studies from neuroscientists since its initial description in the early 1980s (5,6), its clinical significance in man remained enigmatic until L1 mutations were identified in patients with mental retardation and various neurologic disorders (3). The clinical picture resulting from L1 mutations is extremely variable (3,7–12) and includes the syndromes X-linked hydrocephalus due to stenosis of the aqueduct of Sylvius (HSAS), spastic paraplegia type-1, X-linked agenesis of the corpus callosum and MASA syndrome (mental retardation, aphasia, shuffling gait, adducted thumbs) (12,13). These four conditions originally were thought to represent distinct clinical entities, but since L1 mutations were found to be the cause of all of them (14–18), they were lumped together into one clinical condition (10). Since the main symptoms include corpus callosum hypoplasia, mental retardation, adducted thumbs, spastic paraplegia and hydrocephalus, this disorder is now referred to as CRASH syndrome (10). More than 70 L1 mutations in all parts of the L1 molecule have been described in CRASH patients, with almost every family having its exclusive L1 mutation. A continuously updated overview of these mutations is provided at our L1 Mutation Web Page at http://dnalab-www.uia.ac.be/dnalab/l1/ (19).

Recently, two transgenic mouse models with a targeted null mutation in the L1 gene have been generated using embryonic stem cell technology. Dahme *et al.* (20) generated L1 knockout (KO) mice by interruption of exon 8 through insertion of a neomycin/thymidine kinase cassette. These mice were smaller, less viable and less sensitive to pain compared with their wild-type (WT) littermates, and appeared to have weaker hindlimbs, possibly due to hypoplasia of the corticospinal tract. The extent of hydrocephalus was dependent on the genetic background of the mouse strain: when bred on a C57BL/6J background, hydrocephalus was detected upon light microscopic examination of the brain, whereas in the KO mice bred on a

*To whom correspondence should be addressed. Tel: +323 820 2570; Fax: +323 820 2566; Email: fransen@uia.ua.ac.be

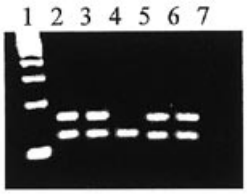

Figure 1. RT-PCR analysis. mRNA was isolated from brain tissue from 1- and 4-day-old mice. RT-PCR with primers 1F and 2R (located in exons 8 and 9, respectively), yields a 164 bp band in controls but not in the KO. As a positive control, RT-PCR products (120 bp) of the murine *Fmr1* (fragile X mental retardation) gene are shown. PCR products from both reactions were spotted together into the same lane. Lane 1, 100 bp length marker; lane 2, heterozygous female (1 day old); lane 3, heterozygous female (1 day old); lane 4, KO male (4 weeks old); lane 5, WT male (4 weeks old); lane 6, WT male (4 weeks old); and lane 7, blank. The KO mouse does not show an L1 RT-PCR product, although the *Fmr1* mRNA signal is present.

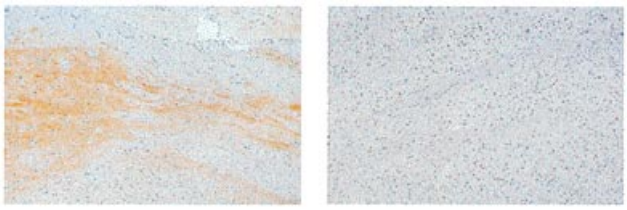

Figure 2. Immunohistochemistry of the brain. Brain slices stained with a commercial rat monoclonal antibody against L1 were analyzed by light microscopy. Sagittal cryostat brain sections (7 μm) from WT (left) and KO (right) mice are shown. Fiber bundles were immunostained for L1 using the indirect immunoperoxidase method. In WT brain sections, some fibers of the internal capsule and the substantia nigra are labeled for L1 (left), whereas all fibers in KO brain are negative for L1 (right). The KO is at magnification ×50, the WT at magnification ×60.

129/SvEv background, no ventricular dilatation was found. In the peripheral nerve system, the interaction between axons and Schwann cells was disturbed. Simultaneously, Cohen *et al*. (21) generated L1 KO mice by replacing exons 13 and 14 of the murine L1 gene, encoding the sixth immunoglobulin domain, by a neomycin/thymidine kinase cassette. The KO mice were bred in a 129/Sv background. Upon western blot analysis on whole-brain lysates, no L1 was detectable in the KO mice, indicating that L1 expression was completely abolished, in contrast to the KO mice generated by Dahme *et al*. (20), that showed a very low (less than a few percent) L1 expression. Like the KO mice generated by Dahme *et al*. (20), the KO mice generated by Cohen *et al*. (21) were less viable and smaller than their littermates. The eyes were smaller and sunken, the fur was abnormal, and the hind-paw toenails abnormally long. Dragging of the hindlimbs occasionally was present. Most of the KO mice did not reproduce. In addition, Cohen *et al*. (21) found a defect in the guidance of corticospinal axons. Hydrocephalus, on the other hand, was not detected upon standard pathological examination.

In this study, we further characterized the brain abnormalities and the behavior of the KO mice generated by Cohen *et al*. (21). Using high resolution magnetic resonance imaging (MRI), subtle abnormalities in the brain and the ventricular system were detected. An abnormality in the cerebellar vermis was further documented using histological techniques. The behavior and cognitive function of the KO mice were studied using a number of standard tests.

RESULTS

RT-PCR analysis

To verify the absence of L1 in the KO mice, we performed nested RT-PCR analysis on total mRNA isolated from the brain of 1-day- or 4-week-old KO mice. This technique allows the detection of extremely low levels of mRNA transcripts. Using primers localized in exons 8–9, proximal to the site where the neomycin cassette had been inserted, and primers annealing in exons 20–21, distal to the insertion site, no RT-PCR product could be detected in the KO mice, in contrast to controls and heterozygotes (Fig. 1).

Immunohistochemistry of the brain

We have stained brain sections with a variety of functional markers specifically staining neurons (MAP-2, β-tubulin, serotonin, synaptophysin, neuron-specific enolase, GAP-43) or glial cells (S100, galactocerebroside). No differences in localization pattern between KO and WT brain sections were found (data not shown).

Cryostat sections from 6-week-old mouse brains were stained with monoclonal antibodies against L1. In normal adult mouse brain, L1 expression was low but present, whereas in brain sections from KO mice, L1 is undetectable (Fig. 2). The same sections were also stained with a monoclonal antibody against NCAM, a cell adhesion molecule homologous to L1. The staining pattern of the NCAM antibody was indistinguishable between the KO and the control mice (not shown).

Impaired neurite growth on L1 substrate

To determine whether neurons without L1 have an impaired ability to extend neurites, dorsal root ganglia (DRG) neurons from KO and WT mice were cultured on laminin, L1–Fc chimera or control substrates (polylysine and anti-Fc antibodies). The L1–Fc chimera, a chimeric molecule consisting of the Fc region of human IgG and the whole extracellular domain of human L1, has been shown to be biologically active in stimulating L1-dependent neurite growth, when affinity coated to tissue culture substrates (22). Both on laminin and on a control substrate of polylysine and anti-Fc antibodies, there were no differences in either the percentage of neurons with neurites or the mean neurite length of KO and WT neurons. This indicates that KO neurons do not have an impaired ability to produce neurites on strong promoters of neurite growth such as laminin or weakly promoting substrates like polylysine coated with anti-Fc antibodies (Fig. 3A).

On L1–Fc, however, KO neurons had a significantly impaired ability to extend neurites compared with WT neurons. Significantly fewer KO neurons showed neurite outgrowth (Fig. 3A; $P < 0.00001$, contingency table analysis), and those neurites that were produced were shorter than those of neurons from WT mice [Fig. 3B; $P = 0.0003$, one-way ANOVA followed by Fisher's protected least significant difference (PLSD)]. Furthermore, the low level of neurite outgrowth from KO neurons on L1–Fc was not

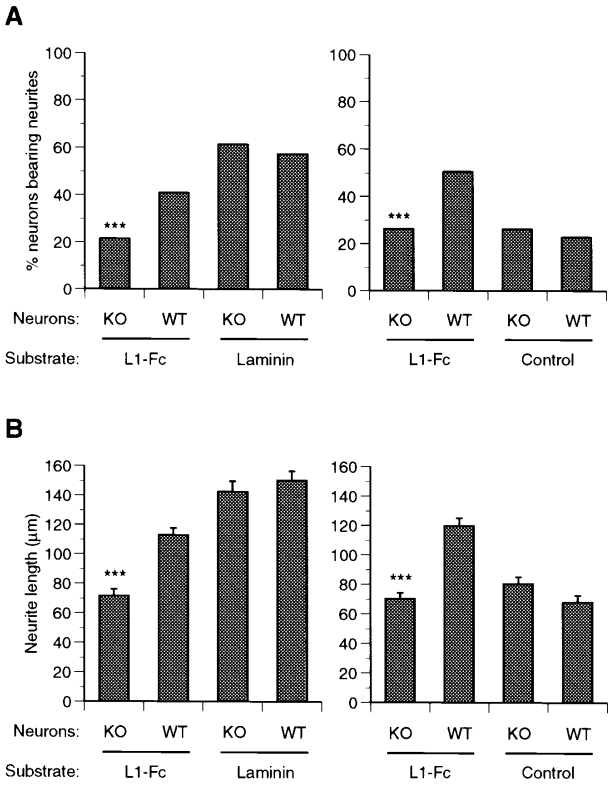

Figure 3. L1-mediated neurite outgrowth in DRG neurons. Neurons were cultured on L1–Fc chimera, laminin or control substrate for 16 h, and neurite growth was analyzed. (**A**) The percentage of neurons that bear neurites is shown. This percentage was not significantly different between KO and WT neurons when growing out on laminin or control substrate, whereas on L1–Fc, the percentage of KO neurons with neurites was significantly smaller ($P < 0.0001$; contingency table analysis). (**B**) The average length (mean ± SEM) of the neurites. Grown on laminin or control sustrate, the neurite length of the KO and WT neurons is not significantly different, whereas on L1–Fc substrate, the neurites from the L1-minus neurons are significantly shorter than the neurites from the WT neurons ($P < 0.0001$; one-way ANOVA followed by *post-hoc* Fisher's PLSD).

significantly different from the outgrowth seen with KO or WT neurons on control substrate. These results indicate that loss of L1 expression in neurons eliminates neurite growth stimulated by L1 substrate. This is consistent with the idea that L1-mediated neurite growth occurs via a homophilic binding mechanism with substrate-bound L1 (23).

Magnetic resonance imaging (MRI) of the brain and the ventricular system

The L1 129/Sv KO mice studied here did not show evidence of hydrocephalus when studied by standard pathological techniques (21) (data not shown). To test for subtle abnormalities in the brain and the ventricular system, we studied the KO mice and their WT littermates by high resolution MRI. This technique allows accurate surface and volume calculations of brain structures using the watershed-based segmentation method (24). Both total brain and cerebellar volumes were significantly reduced in the KO mice compared with WT littermates (Fig. 4A, Table 1), in line with the reduced body weight of the KO mice.

MRI of the ventricular system identified three abnormalities. First, in five out of five KO mice, the shape of the 4th ventricle was abnormal (Fig. 4B, coronal section). Volume calculations showed that the volume of this 4th ventricle was significantly increased in the KO mice compared with WT controls (Table 1). Secondly, we observed a significant dilatation of the lateral ventricles in the KO mice, but not the 3rd ventricle (Table 1, Fig. 4C). Although gross hydrocephalus, comparable with some human patients or with the L1 KO bred on a C57BL/6J background (20), was not present, the dilatation of the lateral ventricles was observed in all five KO mice tested ($P = 0.002$). Third, the shape of the aqueduct of Sylvius was different between KO and WT mice. In mice, the aqueduct, which connects the 3rd and the 4th ventricle consists of two parts: the anterior part ranging from the 3rd ventricle to a fork-like structure called the ampulla, and the distal part connecting the ampulla with the 4th ventricle. This latter part is extremely narrow, and could not be visualized by MRI. Serial coronal sections of the anterior part indicated that this part of the aqueduct was longer in KO mice ($P = 0.002$), suggesting that the distance between the 3rd ventricle and the ampulla was increased. The cross-section of the aqueduct, however, was normal at each section level, and the total volume was not significantly different between the KO mice and the WT littermates (Fig. 5). No indications of stenosis of the aqueduct were found.

Table 1. Estimation of surface area and volume of brain regions by MRI

Parameter	KO ($n = 5$)	WT ($n = 5$)	*P*-value
Surface total brain (mm^2)	61.75 ± 0.82	66.45 ± 1.28	0.021
Surface vermis (mm^2)	8.392 ± 0.15	10.76 ± 0.31	0.0005
Surface ratio vermis/total brain	0.136 ± 0.002	0.165 ± 0.004	0.0007
Volume total brain (mm^3)	460.4 ± 8.9	519.2 ± 7.3	0.002
Volume cerebellum (mm^3)	64.00 ± 1.58	74.20 ± 1.39	0.003
Volume ratio cerebellum/total brain	0.139 ± 0.002	0.143 ± 0.002	0.228
Ventricular volumes (mm^3)			
4th ventricle	0.96 ± 0.06	0.43 ± 0.05	0.0003
4th lateral ventricle	0.61 ± 0.08	0.32 ± 0.06	0.027
3rd dorsal ventricle	0.29 ± 0.04	0.35 ± 0.05	0.421
3rd ventricle (ventral)	0.34 ± 0.03	0.29 ± 0.04	0.362
frontolateral ventricle	0.41 ± 0.04	0.14 ± 0.03	0.002

Variables are indicated as mean ± SEM. *P*-values were derived from a two-tailed Student's *t*-test. Surfaces were estimated on midsagittal sections.

The coronal section through the 4th ventricle (Fig. 4B) suggested that the cerebellum, visible above the 4th ventricle on this section, was abnormal in the KO mice. On a midsagittal brain section (Fig. 4D), the cerebellum of the KO mice seems considerably reduced compared with the rest of the brain. To quantify this, we calculated the ratio between the surface of the cerebellum on the midsagittal section and the surface of total brain on this section. In the KO, the ratio was significantly reduced ($P < 0.0007$).

We also calculated the volume of the cerebellum and the volume ratio cerebellum/total brain. This ratio was not significantly different between KO and WT mice (Table 1). These data

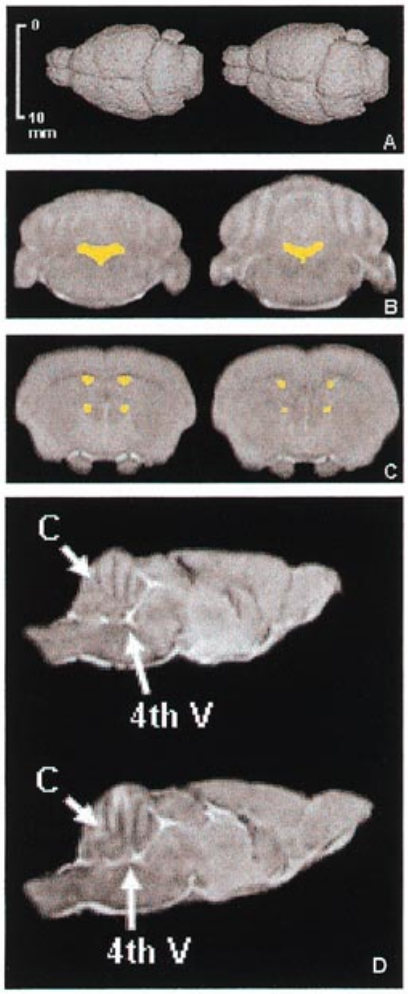

Figure 4. Magnetic resonance imaging (MRI) of the brain. (**A**) 3D reconstructions of brain of a KO (left) and a WT male littermate (right). The KO mice have a smaller brain, and the upper part of the cerebellum seems less developed. (**B**) Coronal MR images of the brain of a KO (left) and a WT littermate (right) through the 4th ventricle, the cerebellum and the pons. The 4th ventricle, indicated in yellow, is dilated in the KO, whereas the cerebellum, which lies above the 4th ventricle, is smaller in the KO than in the WT littermate. (**C**) Coronal MR images of the brain of a KO (left) and a WT littermate (right) through the fronto-lateral ventricles that are visible as four spots. Note the ventricular enlargement in the KO mice. (**D**) Midsagittal MR images of the brain of a KO (top) and a WT littermate (bottom). The 4th ventricle (4V), the aqueduct of Sylvius and the vermis are visible. The cerebrospinal fluid in the ventricular system is brightly lit. The cerebellum (C) appears smaller in the KO and its shape is different.

suggest that in the KO mice, the cerebellar hemispheres as a whole are not hypoplastic relative to the rest of the brain, but that the structure connecting the two cerebellar hemispheres, the cerebellar vermis, is reduced in size.

Histological studies of the vermis

On a midsagittal sections of whole brain (Fig. 6A), and on midsagittal tissue sections counterstained with cresyl violet, the whole posterior part of the aqueduct, including the ampulla and the 4th ventricle (Fig. 6B and C), appeared enlarged in the KO mice.

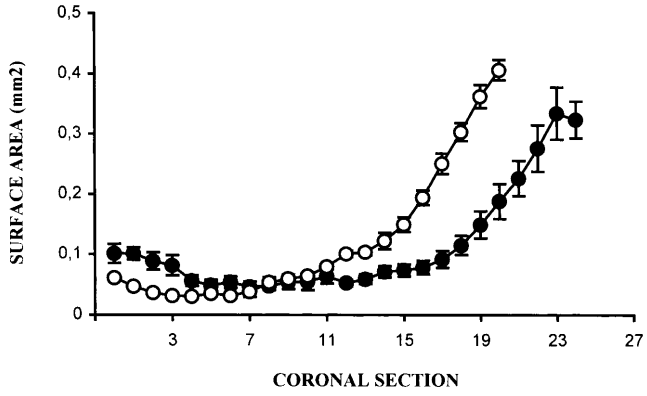

Figure 5. Cross-section of the anterior part of the aqueduct of Sylvius. The mean (SEM) surface area of the anterior part of the aqueduct, between the 3rd ventricle and the ampulla, was calculated on coronal brain sections from KO and WT mice. Sections 1 is situated at the anterior end of the aqueduct. The distance between two sections is 80 (m. In the KO mice, this part of the aqueduct was longer than in the WT mice, but not stenotic. The distal part of the aqueduct, between the ampulla and the 4th ventricle, could not be visualized by MRI.

In five adult KO mice and five adult WT littermates, we determined the surface area of the cerebellar vermis and compared it with the surface area of the cerebral cortex. The average surface area of the cerebral cortex of the KO mice was not significantly different from that of the WT mice (not shown). However, the average surface area of the vermis of the KO mice (7.6 ± 0.2 mm^2) was significantly smaller ($P < 0.001$; *t*-test) than that of the WT mice (8.9 ± 0.2 mm^2). The ratio between the surface areas of the vermis and the cerebral cortex was significantly smaller in the KO mice ($P < 0.02$; *t*-test). This confirms that in the KO mice, the cerebellar vermis is specifically reduced in size compared with the rest of the brain. Interestingly, the vermis hypoplasia appears to be most prominent in lobule 6. In all KO mice tested, one or two of the three sublobules of this lobule were underdeveloped or totally missing (Fig. 6B and C, asterisk), a finding never observed in WT mice. These macroscopic abnormalities in the vermis prompted us to investigate the cytology of the cerebellar cortex, but no microscopic abnormalities could be found (data not shown).

Behavioral tests

Several experiments were performed to analyze the behavior of KO mice. In the wire suspension test, a test for muscle strength, KO mice performed equally well as their WT littermates. The KO ($n = 15$) and the WT ($n = 12$) mice had no problem hanging from the wire for 60 s.

Cage activity, expressed as the number of beam crossings in a standard cage during a 2 h period, demonstrated hypoactivity in KO mice. Ten KO mice displayed 772 ± 184 beam crossings, which is significantly lower than the 1498 ± 142 crossings observed in the group of 18 WT mice ($P = 0.005$).

The rotarod test is a classical test where the mice have to keep their balance on a rotating rod. Five 2-min trials were performed. Each time the mouse falls off, it is placed back onto the rod for a maximum of three attempts per trial. The WT mice ($n = 12$) stayed on the rod during all five trials, whereas most of the KO

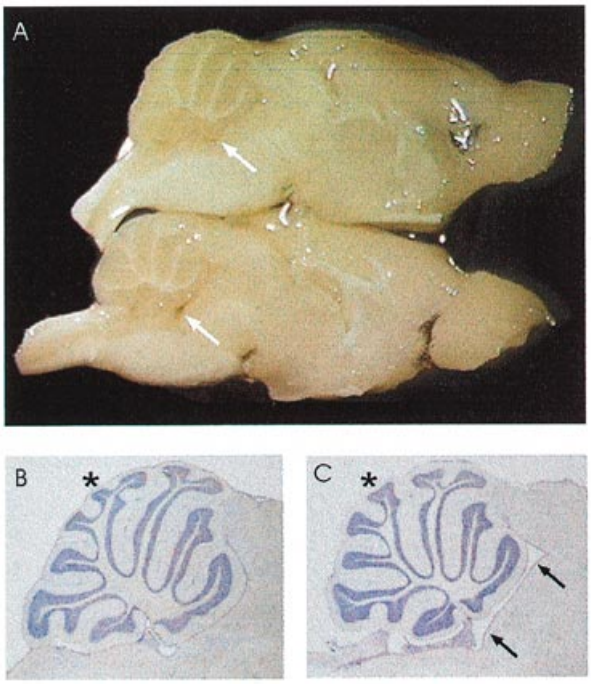

Figure 6. Light microscopic image of a midsagittal section through the brain. (**A**) Whole brain section of a WT (top) and KO (bottom) brain. The size of the vermis is smaller in the KO, whereas the 4th ventricle (white arrow) of the KO is larger than that of the WT. (**B** and **C**) Cresyl violet staining of a midsagittal section through the vermis illustrating the vermis hypoplasia, particularly lobule 6 (asterisk), which is located immediately posterior of the fissura prima, is hypoplastic. Furthermore, the ampulla of the aqueduct of Sylvius (upper black arrow), the posterior part of the aqueduct between the ampulla and the 4th ventricle, and the 4th ventricle itself (lower black arrow) are enlarged in the KO mice, which may be a consequence of the hypoplasia of the vermis.

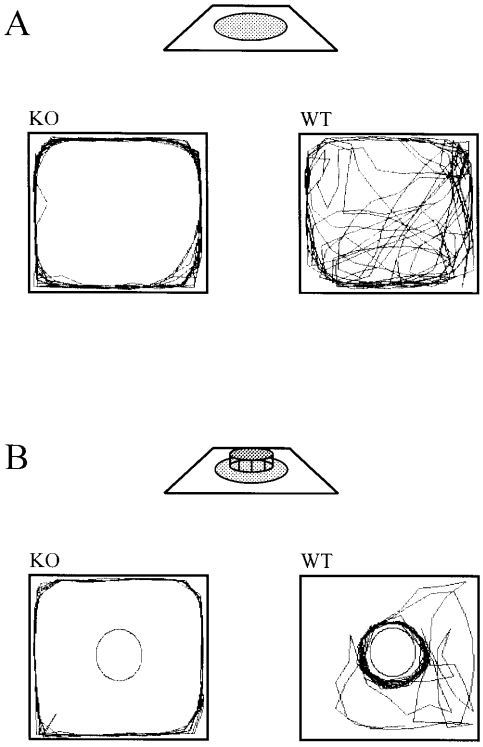

Figure 7. The open field (**A**) and social exploration test (**B**). The 50×50 cm^2 arenas with a 35 cm center circle (A) or imaginary 20 cm annulus around the cage (B) are schematically drawn, and the typical paths of a KO and WT mouse are shown. In both tests, KO mice walked around in a stereotype movement without any tendency to explore either the center of the field or the cage containing two female mice. Path lengths of KO and WT mice were not significantly different; in the examples shown here, path lengths of 2491 and 2281 cm were recorded for the KO mouse and the WT littermate, respectively, in the open field test, and of 1261 and 1513 cm, respectively, in the social exploration test.

mice (n = 15) failed at least at one attempt during the first trial. From the second trial onward, both WT and KO no longer fell off. However, upon visual inspection, the KO mice clearly displayed more difficulties in keeping their balance. Apparently, there was no evidence for gross motor impairments or severe ataxia.

The open field test assesses the behavior of the mice in an empty 50×50 cm Plexi cage during 10 min (Fig. 7A). We observed a dramatic difference in walking pattern between the two groups. The WT controls (n = 19) actively explored the cage, frequently crossing the center of the cage, whereas the KO mice (n = 12) were less inclined to explore the center of the field. Most KO mice, instead, were running in circles (Fig. 7), whereas a few of them 'froze' when put into the open field. The number of entries into the center, which we defined as an imaginary circle with 30 cm diameter in the middle of the cage (Fig. 7A), was significantly lower in KO mice (0.6 ± 0.4) than in the WT group (8.4 ± 2.2; P = 0.01).

The social exploration test is a variant on the open field test with a small round cage with two clearly visible female mice placed in the middle of the large Plexi cage (Fig. 7B). Here too, a qualitative difference in walking pattern was noticed. The WT mice (n = 19) walked frequently around the cage containing the two female mice, sniffing and exploring the females and poking their noses through the bars. They spent 45 ± 7% of their path within a 10 cm radius around the cage. In contrast, KO mice (n = 11) did not adapt their exploration strategy to the extra stimulus provided by the central cage with the female mice. Most of them showed the same stereotype peripheral circling as in the open field test without the females in the center (Fig. 7B), spending only a mean of 3.3 ± 2.4% of their path around the cage (P < 0.0001). In the open field test and in the social exploration test, the mice walked along the wall without actually touching it. In both tests, the path length was not significantly different between the KO and WT group.

Experiments for memory and cognitive function

To test for severe memory deficits, a passive avoidance test was performed using the two-compartment step-through box. During this test, the mice are put into a small, brightly lit compartment. After 5 s, a sliding door to a dark compartment is opened. Upon entrance into this dark compartment, the mouse receives a weak electric shock. Twenty four hours later, the procedure is repeated. A mouse with functional memory will remember the electric shock and will not enter the dark compartment again. The L1 KO mice (n = 5) performed the task as well as the WT mice. None of the KO or WT mice re-entered the dark compartment (cut-off = 5 min), indicating that avoidance learning is not severely affected.

Spatial learning was tested in the Morris water maze (MWM) task, in which the mice have to learn to find a hidden platform in

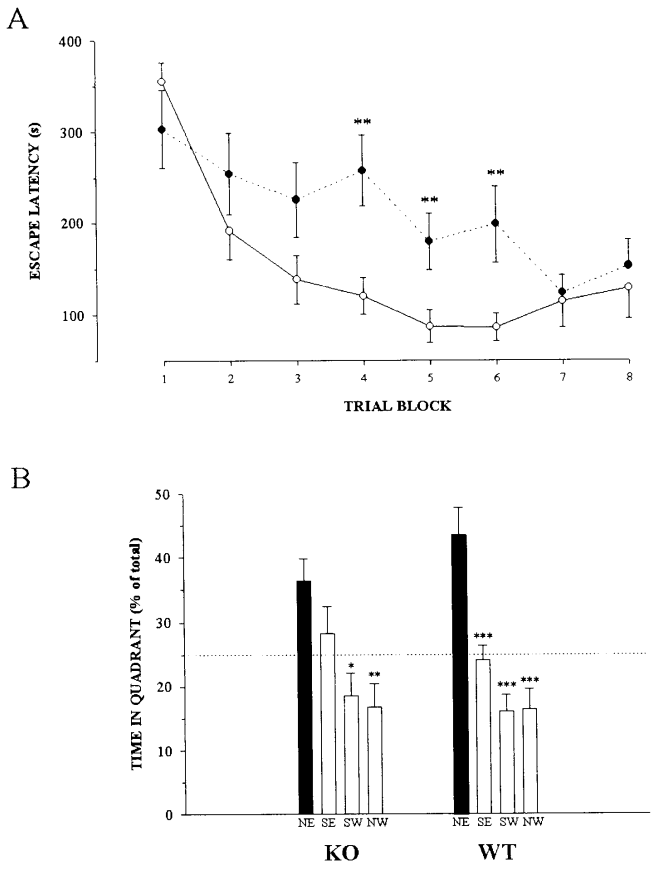

Figure 8. Acquisition (A) and probe trials (B) of the hidden-platform Morris water maze test. (**A**) The escape latency learning curve shows slower acquisition rate in KO mice (closed circles) as compared with WT littermates (open circles). Asterisks indicate the significance of differences between KO and WT latencies: *$P < 0.05$; **$P < 0.01$; ***$P < 0.001$. (**B**) Time spent in the four quadrants of the pool during the probe trial. The platform used to be located in the north-east (NE) quadrant. The significance of the differences between the time spent in the NE target quadrant (black bars) and in the SE, SW and NW quadrants (light bars) is indicated by asterisks. The time that the KO spend in the NE quadrant is not significantly different from the time they spend in the adjacent SE quadrant. All data are means ± SEM.

a circular pool guided by distal visual cues (29). In the acquisition trials, during which the platform is located in a fixed place, we observed that the L1 KO mice ($n = 10$) were capable of learning to find the platform, albeit at a slightly slower learning rate than the WT littermates ($n = 19$) ($P = 0.005$, repeated measures ANOVA; Fig. 8A). However, as the swimming velocity in the KO group was lower than in the WT group ($P = 0.015$, repeated measures ANOVA), we cannot exclude that the difference in escape latency is, at least partly, due to a difference in swimming speed rather than a learning defect.

After the final acquisition trial, the platform was removed and we performed a probe trial, where we measured the time that the mice spent in the quadrant where the platform used to be (target quadrant). WT controls spent the major part of their time in this target quadrant, whereas KO mice did not spend more time in the target quadrant than in the adjacent quadrant (Scheffe F-test; Fig. 8B). Moreover, the KO mice also made significantly ($P = 0.029$) fewer entries in the target area (3.6 ± 0.7) as compared with the control group (7.2 ± 1.1). The swimming speed of KO and WT mice was not significantly different during the probe trial, excluding the possibility that the observed differences are due to motor incapacity.

As most KO mice exhibited stereotype peripheral circling in the open field and social exploration tests, we compared the searching strategies of the mice in the MWM task during the first acquisition trial and the first trial at day 5. Initially, the paths of both the KO (60 ± 4%) and the WT (71 ± 3%) mice were located mainly in the periphery of the circular maze, arbitrarily defined as within 25 cm of the pool wall. At day 5, the searching pattern of the WT mice had changed, and they spent much less time in the periphery of the pool (33 ± 6% of their path). In the KO mice, on the contrary, 62 ± 8% of their path was still localized in the periphery ($P < 0.01$).

DISCUSSION

Several biochemical and cell biological studies have highlighted the vital role of L1 in processes such as axon outgrowth and neuronal migration during brain development. Mutations in L1 in humans result in a combination of X-linked mental retardation and neurologic abnormalities including hydrocephalus, spasticity and hypoplasia of the corpus callosum (CRASH syndrome). Although the clinical spectrum of L1-associated disease is well known, the link between L1 dysfunction and the pathogenesis of CRASH syndrome is still unclear. Therefore, two groups recently have generated transgenic mice with a knockout in the L1 gene (20,21), and studied the mice using mainly histological and pathological techniques. Here we have characterized further the mice generated by Cohen *et al.* (21), focusing on brain structure, behavior and cognitive function.

The general characteristics of both L1 KO mice include reduced viability and reproduction, reduced weight, sunken and lacrimous eyes, fur abnormalities and long toenails of the hind-paws. Abnormalities of the hindlimbs were also noticed, which is probably correlated with the hypoplasia of the corticospinal tract (20). These abnormalities might be equivalent to the spastic paraparesis of the lower limbs in human patients, that also show hypoplasia of the corticospinal tract (11). It is most likely that a defect in the guidance of corticospinal axons underlies the corticospinal tract hypoplasia (21), which corresponds to the *in vitro* data obtained by us and by Dahme *et al.* (20) showing that neurite outgrowth is impaired in L1-deficient neurons.

Using MRI, we observed abnormalities of the ventricular system and vermis hypoplasia in the KO mice. Recently, a neuroradiological study on human patients pointed out that hypoplasia of the vermis is a consistent abnormality in CRASH syndrome (8). In the L1 KO mice, we found a specific size reduction of the cerebellar vermis, most notably in the 6th cerebellar lobule. The layering of the cerebellar cortex did not show cytological abnormalities, which parallels the observations made in human patients (25). The severity of hydrocephalus in human patients ranges from marginal widening of the lateral ventricles and sometimes the 3rd ventricle, to a massive ventricular dilatation and macrocephaly, often resulting in pre- or perinatal death (9,26,27) . In the ventricular system of our L1 KO mice, we found a mild dilatation of the lateral and the 4th ventricles, but not of the 3rd ventricle. These observations raise the question of why and how loss of L1 produces hydrocephalus

of the lateral ventricles in mice. One explanation is based upon our observation that loss of L1 has a clear effect on the L1-mediated neurite outgrowth of cultured neurons (20) and the well-known role of L1 in axon pathfinding (28). In the absence of L1, neurons that project through the corpus callosum or corticospinal tract fail to make proper connections and die, which results in loss of cortical gray and white matter. The dilatation of the lateral ventricles could therefore be a form of hydrocephalus *ex vacuo*. A second possibility, supported by the evidence that L1 is responsible for axon fasciculation, is that the loss of L1-mediated adhesion between axons in the white matter of the cortex leads to an increase in brain compliance, which would lead directly to an increase in ventricle size, even with a normal cerebrospinal fluid pressure. Although these two hypotheses are amenable to testing, they cannot explain the occurrence of high pressure hydrocephalus in some human CRASH patients.

A third possibility is that the primary cause of the hydrocephalus is the altered shape of the aqueduct of Sylvius. This altered shape may render the drainage of the cerebrospinal fluid less efficient, leading to the mild ventricular dilatation seen in our L1 KO mice, and reminiscent of the clinical picture of some mildly affected CRASH patients. Possibly, as the aqueduct is longer than normal, it may be more vulnerable to obstruction. If the aqueduct indeed becomes stenotic, fluid pressure will build up in the lateral ventricles and result in gross hydrocephalus, reminiscent of the situation observed in the L1 KO mice bred in a C57BL/6J background (20) and in severely affected human patients. Factors such as modifier genes or genetic background may influence the aqueduct stenosis and determine whether the mild ventricular dilatation, caused by the absence of L1 alone, ends up in massive hydrocephalus.

The dilatation of the 4th ventricle probably has a different origin than in the lateral ventricles. The 4th ventricle lies immediately adjacent to the cerebellar vermis (29), and the dilatation of the 4th ventricle may be a direct consequence of the vermis hypoplasia. Therefore, the dilatation of the 4th ventricle probably represents hydrocephalus *ex vacuo*, where the increase in ventricle size is caused by the loss of brain parenchyma, in this case a decrease in the size of the vermis (see also Fig. 6A). Similarly, the altered shape of the aqueduct of Sylvius may also be due to the vermis hypoplasia as the vermis also lies in close proximity to the aqueduct and the ampulla (Fig. 6B and C).

The study of the brain and the ventricular system has been helped greatly by the use of MRI. Although this technique is now used routinely in clinical medicine, MRI studies on transgenic mice are scarce in spite of some clear advantages over histopathological studies. Pathologic studies are prone to artifacts induced by dehydration and fixation procedures, which is a major problem if, for example, a mild ventricular dilatation in mice is suspected. For instance, in our studies, the calculated surface area of the vermis on histological sections is >10% smaller than the surface of the vermis that was calculated using MRI. Also, MRI is performed upon living animals, and it allows qualitative and quantitative studies of brain structure or any other organ, while it is fully functioning. Here, it allowed accurate *in vivo* imaging and volume calculations of the brain and the ventricular system that would not have been possible using standard pathological techniques, and they revealed subtle abnormalities that were not detected in previous studies.

The behavior of the KO mice was characterized by stereotype peripheral circling. In the open field test, the mice constantly ran along the walls of the cage, without exploring the inner part of the cage. Even in the social exploration test, where control male mice focus on the cage with the female mice, most KO mice show the same stereotype peripheral circling. Stereotype peripheral circling might have influenced the performance of the KO mice in the MWM task. Since exploration is crucial for the acquisition of this task, impaired exploration, as displayed by the KO mice, could therefore have interfered with acquisition.

Spatial learning defects as evidenced by impaired performance in the MWM previously have been attributed to defective hippocampal long-term potentiation (LTP) (30,31). However, electrophysiological experiments revealed no LTP abnormalities in the KO mice (J.-M. Godfraind, personal communication).

Therefore, and in view of the vermis hypoplasia, it is tempting to speculate that the cause of the spatial impairment and the abnormal behavior is related to the cerebellar abnormalities. Several authors have proposed that the computational properties of the cerebellum are not only important in motor functions, but are also involved learning and other cognitive functions, including a distinct role in the processing of spatial information (32–35). Recent findings by Petrosini *et al*. (36) showed that surgical removal of hemicerebellum and hemivermis in rats leads to striking behavioral changes. In the MWM, rats with cerebellar lesions were completely unable to develop useful maze exploration strategies, and were constantly circling along the walls of the pool. Their circling pattern was very similar to the stereotype peripheral circling we have observed in our KO mice during the open field tests. However, in contrast to the rats with hemicerebellar and hemivermis lesions, the vermis abnormalities in our L1 KO mice were located predominantly in the 6th cerebellar lobule. This area of the cerebellum, which is part of the oculomotor vermis, controls saccadic eye and head movements (37), and is therefore necessary for an adequate exploration of the external world. It may therefore be that the KO mice cannot explore their surroundings properly due to the vermis hypoplasia, and that the stereotype peripheral circling is a consequence of this.

In conclusion, the L1 KO mice show evidence of abnormalities that are compatible with the clinical symptoms of human patients with CRASH syndrome: defects in the corticospinal tract, a variable degree of hydrocephalus, hypoplasia of the vermis and learning deficiencies. The mice will allow further characterization of the abnormalities associated with L1 dysfunction, which may shed new light on the fundamental causes of these abnormalities. Although the nature of the vermis hypoplasia remains to be investigated, it has focused attention on the role of L1 in cerebellar development. The impaired exploration patterns of the KO mice, which may be due to the vermis hypoplasia, have highlighted the possible role of the cerebellum in the processing of spatial information. Understanding the cellular mechanisms that contribute to these defects will be facilitated by this animal model.

MATERIALS AND METHODS

RT-PCR analysis

For nested RT-PCR, total mRNA was isolated from the brain of 1-day- or 4-week-old mice using the TRIzol™ Reagent (Gibco BRL) followed by reverse transcription into total cDNA using the Superscript™ Preamplification System (Gibco BRL). The nested RT-PCR analysis was performed, using two different primer sets. The first nested RT-PCR was performed with primers annealing

proximal to the site of the neomycin insertion. The outer PCR was performed using primers 2F (5′-CAATCATTCAGACTA-CATCTGC-3′, exon 6) and 5aR (5′-CTTCATCCAGCCACTG-GACAC-3′, exon 12). The PCR product was diluted 1/50 and the inner PCR was performed on 1 µl of this diluted product using primers 1F (5′-GTGGGCGAAGAGGACGATGG-3′, exon 8) and 2R (5′-CTTGGCAGTCTAGGCGGGC-3′, exon 9). The second nested RT-PCR was performed with primers annealing distal to the site of the neomycin insertion. The outer PCR was performed using primers 4bF (5′-GAGATCAAAGTCCAGG-CAG-3′, exon 18) and 5bR (5′-CTCATATTTGG-TGTCAGGC-3′, exon 24). The PCR product was diluted 1/50 and the inner PCR was performed on 1 µl of this diluted product using primers 5bF (5′-CACAGCAAGAGGCATATCC-3′, exon 20) and 4bR (5′-CAGGGTGGCCAGGCACTC-3′, exons 20–21). Primers S1 and S2, amplifying part of the fragile X gene, were used as a positive control (38).

Immunohistochemistry of the brain

Brains were obtained from 6-week-old mice (two KO and two WT males). Immediately after dissection, brains were snap-frozen in liquid nitrogen and stored at –80 °C. Cryostat sections (8 µm) were cut with a Leica CM3000 and fixed with 3% buffered paraformaldehyde for 10 min, followed by a methanol step for 20 min. Endogenous peroxidases were inhibited by a 30 min incubation in phosphate-buffered saline (PBS)–hydrogen peroxide–sodium azide solution. Subsequently, sections were incubated with rat monoclonal antibodies against either L1 or NCAM (Boehringer Mannheim). Antigen–antibody complexes were visualized with rabbit anti-rat IgG conjugated with horseradish peroxidase (Dako, Denmark), supplemented with 2% normal mouse serum to block cross-reactivity with mouse immunoglobulins. Finally, peroxidase activity was visualized by an incubation with buffered 3,3′-diaminobenzidine-HCl as a substrate.

Neurite outgrowth of KO neurons

Generation of L1–Fc chimeric protein. A chimeric molecule consisting of the Fc region of human IgG and the whole extracellular domain of human L1 was constructed using the pIg-tail expression system (Novagen, Madison, WI). A cDNA encoding the extracellular domain of L1 was obtained by PCR from the pBluescript II KS+ which contains a cDNA encoding the full-length human L1 in its *Hin*dIII–*Eco*RI site (12). Primers used for the PCR amplification were as follows: a sense primer corresponding to nucleotides 2901–2918 of the L1 cDNA; and an antisense primer 5′-TCGCGAATTCACTTACCTGTAGGGAG-CCTCACGCGGCCTG-3′. The latter primer contains a cDNA fragment (bp 3320–3339) encoding for the C-terminal end of the L1 extracellular domain, which is immediately followed by a splice donor sequence and an *Eco*RI restriction site. The PCR product was digested with *Bsi*wI (located at bp 3015) and *Eco*RI, and ligated into a *Bsi*wI–*Eco*RI-digested pBluescript containing the full-length L1 cDNA. A *Hin*dIII–*Eco*RI fragment of the resulting plasmid, which contains a cDNA encoding the L1 extracellular domain followed by a splice donor sequence, was then ligated into a *Hin*dIII–*Eco*RI-digested pIg vector. The PCR-amplified region and the insert–vector junctions were confirmed by sequencing. COS-7 cells were transfected with the pIg vector using Lipofectamine™ reagent according to the manufacturer's protocol (Gibco BRL, Gaithersburg, MD). A culture supernatant of the transiently transfected COS-7 cells was used in the present study. The chimeric protein isolated by a protein A–Sepharose column was confirmed to have an expected molecular weight of 250 kDa by silver staining.

Culture of dorsal root ganglia (DRG) neurons and neurite growth assay. KO and WT male mice (3–6 months old) were killed by over-anesthesia with Metophane™. The DRG neurons were dissected and trimmed to remove spinal nerves and then incubated in 0.25% collagenase A (Boehringer Mannheim, Indianapolis, IN) in Dulbecco's modified Eagle's medium (DMEM) (Gibco BRL) containing 10% fetal bovine serum (FBS) for 1.5 h at 37 °C. After trituration, the DRG neurons were incubated in the presence of 0.1 mg/ml DNase (Boehringer Mannheim), and were again triturated until a single cell suspension was obtained. After centrifugation, the cells were resuspended in DMEM with 10% FBS and 50 ng/ml nerve growth factor (NGF), and were plated on two-chamber plastic slides (Lab-Tek, Naperville, IL) at a density of ~1000 cells/cm^2. The culture slides had been pre-coated with one of the following three substrates: laminin (sequentially coated with poly-L-lysine and 10 µg/ml laminin), L1–Fc (sequentially coated with poly-L-lysine, 20 µg/ml Fc-specific goat anti-human IgG and L1–Fc chimera) and control substrate (sequentially coated with poly-L-lysine and 20 µg/ml Fc-specific goat anti-human IgG). The cells were fixed at 16 h after plating, and images of the cells were obtained using the Image-1/MetaMorph Imaging System (Universal Imaging, West Chester, PA). Neurite length was measured as the distance between the tip of the longest neurite and the periphery of the cell soma where the neurite emerges. Only the neurites that met the requirements described previously (23) were included in this study.

Magnetic resonance imaging (MRI)

MR imaging. *In vivo* MRI was performed on an MR microscope (SMIS, Guildford, UK) with a 7T horizontal bore magnet and 8 cm aperture self-shielded gradients with a strength of 0.1 T/m (Oxford Instruments). By means of a stereotactical apparatus—ear plugs and a tooth bar—the head of the anesthetized mouse was firmly fixed and positioned in the center of a 30 mm wide radio frequency bird cage coil—used for both transmitting and receiving. Sagittal scouting spin echo images were acquired to guide the positioning of the mouse head in the center of the magnet. To obtain high-resolution coronal slices of the mouse brain within reasonable experimental time, a 3D Fast Spin Echo sequence (39) was used with an echo train length of four, reducing the imaging time by a factor of 4. MR signals of a 3D volume of 20×20×22 mm^3 were acquired within a 256×128×64 matrix. The images were taken with a repetition time of 2500 ms and an echo time of 35 ms. The central line of the k-space was sampled at the first echo. These parameters were chosen to obtain 3D images of the brain with optimal contrast between the ventricles and the surrounding brain tissue, within an acceptable time. The MR data were reconstructed to an image matrix of 256×256×256 containing 256 coronal slices of 80 µm with spatial resolution of 78×78 µm^2.

Data processing. Surface areas from different sections through the brain, and volumes from different brain structures, were estimated to find differences between KO and WT mice. All image processing was performed on an HP 720 workstation.

Surface areas were determined on coronal and midsagittal brain sections. To extract quantitative volume information from a set of *in vivo* obtained images of the mouse, a semi-automatic 3D segmentation technique (24) was applied on the 3D MR images data set. The volumes of total brain and cerebellum were estimated. The cerebellum was delineated as the brain structure dorsal to the aqueduct and the 4th ventricle on a midsagittal section. The volumes of the different ventricular structures were segmented and determined from the same 3D sets of coronal MR images. MRI parameters were chosen in such a way that an apparent intensity distinction was obtained between the ventricles and the surrounding tissues which allowed an easy segmentation of these structures based on threshold selection. For each data set, the threshold was derived consistently from the histogram of the total brain-segmented data. Ventricular structures were defined on coronal MR images, according to the Mouse Brain atlas (29). Their position was defined in terms of antero-posterior distance to the interaural line: (i) lateral 4th ventricles: high intensity structure from IA –3.40 to –1.88 mm as located lateral to the 4th ventricle defined at IA –2.00 mm; (ii) 4th ventricle: high intensity structure positioned at the midline from IA –3.40 mm to –1.54 mm; (iii) dorsal 3rd ventricle: segmentation started caudally as a dorsal narrow line or spot with high intensity on the image slice that displayed the mammillary recess 3rd ventricle at IA 1.10 mm, and proceeded to IA 1.50 mm where this structure spread out more laterally ending as a spot at IA 3.70 mm, always well-separated from the 3rd ventricle; (iv) 3rd ventricle: segmentation started as a ventrally located spot at IA 1.10 mm, proceeded as a vertical line finally ending as a ventral spot at IA 4.18 mm; and (v) lateral ventricles were only partly segmented from IA 3.10 to 4.98 mm, as segmentation of the ventro-lateral part of the ventricles was very difficult. The surface area of the anterior part of the aqueduct of Sylvius was calculated on serial coronal sections from the 3rd ventricle to the ampulla of the aqueduct. The posterior part of the aqueduct, from the ampulla to the 4th ventricle, could not be visualized. Values are indicated as means ± SEM, and statistical analyses were performed with a two-tailed Student's *t*-test, unless otherwise stated.

Histology of the vermis

To investigate the surface areas of different brain regions in sections, five adult L1 KO mice and five adult WT littermates were anaesthetized with a mixture of ketamine (50 mg/ml) and xylazine (2.8 mg/ml) in sodium chloride (3.6 mg/ml); and perfused transcardially with standard paraformaldehyde–glutaraldehyde fixatives (40). The brains of the animals were removed, cryoprotected in sucrose, embedded in gelatin and cut sagitally on a cryotome in 40 μm sections. Subsequently, all sections were mounted on glass slides, counterstained with cresyl violet and coverslipped. The surface areas of the vermis of the cerebella (midsagittal plane) and the cerebral cortices (parasagittal plane, 1 mm from the midline) were measured with the use of an automated Neurolucida System (MicroBrightField). Of each area of each animal, four sections were investigated, and the values were averaged per animal.

Neurologic, behavioral and cognitive function tests

Male KO mice and male WT littermates were used. Behavioral testing began when mice were 3 months old, and finished within 3 weeks.

Wire suspension and rotarod tests were used to assess basic neuromotor functions of the animals. In the wire suspension test of grip strength, the front paws of the mouse were put on a taut horizontal steel wire (0.6 mm thick), 46 cm above a table top. Only one trial was performed, during which the animal had to hang onto the wire with front paws only, and the latency until falling was recorded up to a maximum of 60 s. Motor coordination and equilibrium were tested on the rotarod apparatus. Each mouse was placed on a rotating PVC rod (6 r.p.m.) for four test trials with an intertrial interval of 10 min. The time on the rod was recorded up to 120 s cut-off.

Cage activity of the mice was assessed using a standard laboratory mouse cage (16×22 cm^2) placed between three infrared beams (two perpendicular to the long axis and one perpendicular to the short axis), which were connected to a lab-built microprocessor counter. The mice were placed in the cage for 2 h, during which beam crossings were counted.

Open field behavior was assessed in a brightly lit square arena (50×50 cm^2). Mice always started from the same corner of the arena, and were allowed a 1 min adaptation period. Their path was recorded for 10 min using a computerized video tracking system (San Diego Instruments, CA) to measure dwells and entries of the animals in different imaginary parts of the field; measures include entries in the four 7×7 cm^2 corner squares, entries in the circle (diameter 35 cm) and time spent in the center versus the periphery of the field. Both cage and open field activity were assessed in mice on reversed dark–light cycle during their dark phase.

Social exploration was assessed using the open field set-up with a 15 cm round cage in the middle of the arena. Two female Swiss albino mice were put in the cage, and the test mouse was introduced in the arena for a 10 min recording of movements. Movements of the test animal were recorded using the video tracking system; the main exploration measures were entries and path length in the imaginary 10 cm annulus around the cage. A few of the animals in both groups froze upon introduction into the open field and social exploration arenas, and hardly moved at all; such animals were not excluded from the analysis which added to the relatively large variance in recorded parameters.

Passive avoidance learning was tested in a two-compartment step-through box. Animals were put in a small (5×9 cm^2) brightly lit compartment. After 5 s, the sliding door was opened leading to the large (20×30 cm^2) dark compartment. Upon entrance into the dark compartment, the door was closed and animals received a slight electric foot shock (0.3 mA, 1 s). Twenty four hours later, the experiment was repeated, and the time the animals stayed in the small compartment was measured up to 300 s.

A Morris-type water maze task was employed to compare spatial learning abilities between knockouts and controls, as previously described (38). Eight acquisition trial blocks (consisting of four trials randomly starting from one of four positions) were followed by a final 100 s probe trial. The maze used consisted of a circular gray plastic pool (diameter 150 cm, height 30 cm) filled with opacified water and maintained at 26°C. A round Perspex platform (diameter 15 cm) was placed inside the

pool at the center of the north-east (NE) quadrant. The platform was placed 1 cm below the water surface. Animals performed one trial block daily consisting of four swimming trials randomly starting from one of the four positions (N, E, S, W) with 15 min between separate trials. If the animals could not find the platform within the maximum swimming time of 120 s, they were placed on the platform, and had to stay there for 15 s before removal. Between trials, animals were put under an infrared lamp to avoid hypothermia. Eight acquisition trial blocks were followed by a probe trial during which mice had to swim for 100 s in the pool without a platform. During acquisition and probe trials, the movements of the animals in the pool were tracked using a computerized video-tracking system (San Diego Instruments). This system was also used to analyze the searching strategy of the mice, during which the percentage of the path of the mice within the outer section of the circular MWM (the area within 25 cm of the wall) was calculated on the first trial of the first day, and on the first trial of the fifth day of the acquisition. All values are means ± SEM, and all statistical analyses are performed with a two-tailed Student's *t*-test, unless otherwise stated.

Animal handling and dissection

Animals were maintained in our animal facility at a 12 h light–dark cycle, at a constant temperature and humidity. Food and water were supplied *ad libitum*. The animals were treated according to the guidelines of the ethical committee of the University of Antwerp which approved the study protocol.

ACKNOWLEDGEMENTS

We are grateful to M. Van der Heyden and F. Dierickx for animal care, N. Aerts and R. Bernaerts for secretarial assistance, A. Goffinet, E. De Leenheir, J.-P. Bogers, E. Van Marck and J.-P. Timmermans for pathological studies, F. Franck, G. Cheng, Z. Miao and M. Pendergast for technical assistance, M. Van Goethem for RX studies, P. Parizel and M.L. Hlavin for useful discussions, J.A. Kauer, P.F. Maness and J.-M. Godfraint for information on electrophysiologic studies and San-Ho Correwyn and Tom deVries-Lentsch for photographic work. This work was partly supported by a Concerted Action of the University of Antwerp to G.V.C. and P.J.W., a grant of the Flemish Fund for Scientific Research (FWO) to P.J.W., a grant from the Association Française contre les Myopathies (AFM) to P.J.W., a grant of the FWO to P.P.D.D. (G. 0027.97) and NIH grants HD24875 and HD25326 to P.S. H.K. and V.L. were supported by NIH grants EY05285, NS34252 and PO1NS32779. C.I.D.Z. was supported by the Life Sciences Foundation (SLW # 805-33-310), which is subsidized by The Netherlands Organization for Scientific Research. G.V.C. and R.D.H. hold postdoctoral positions with the FWO.

REFERENCES

1. Brümmendorf, T. and Rathjen, F.G. (1995) Cell adhesion molecules 1: immunoglobulin superfamily. *Protein Profile*, **2**, 963–1056.
2. Hortsch, M. (1996) The L1 family of neural cell adhesion molecules—old proteins performing new tricks. *Neuron*, **17**, 587–593.
3. Fransen, E., Van Camp, G., Vits, L. and Willems, P.J. (1997) L1-associated diseases: clinical geneticists divide, molecular geneticists unite. *Hum. Mol. Genet.*, **6**, 1625–1632.
4. Scholey, A.B., Mileusnic, R., Schachner, M. and Rose, S.P.R. (1995) A role for a chicken homolog of the neural cell adhesion molecule L1 in consolidation of memory for a passive avoidance task in the chick. *Learning Motiv.*, **2**, 17–25.
5. Lindner, J., Rathjen, F.G. and Schachner, M. (1983) L1 mono- and polyclonal antibodies modify cell migration in early postnatal mouse cerebellum. *Nature*, **305**, 427–430.
6. Rathjen, F.G. and Schachner, M. (1984) Immunocytological and biochemical characterization of a new neuronal cell surface component (L1 antigen) which is involved in cell adhesion. *EMBO J.*, **3**, 1–10.
7. Willems, P.J., Brouwer, O.F., Dijkstra, I. and Wilmink, J. (1987) X-linked hydrocephalus. *Am. J. Med. Genet.*, **27**, 921–928.
8. Yamasaki, M., Arita, N., Hiraga, S., Izumoto, S., Morimoto, K., Nakatani, S., Fujitani, K., Sato, N. and Hayakawa, T. (1995) A clinical and neuroradiological study of X-linked hydrocephalus in Japan. *J. Neurosurg.*, **83**, 50–55.
9. Schrander-Stumpel, C., Höweler, C., Jones, M., Sommer, A., Stevens, C., Tinschert, S., Israel, J. and Fryns, J.P. (1995) Spectrum of X-linked hydrocephalus (HSAS), MASA syndrome, and complicated spastic paraplegia (SPG1): clinical review with six additional families. *Am. J. Med. Genet.*, **57**, 107–116.
10. Fransen, E., Lemmon, V., Van Camp, G., Vits, L., Coucke, P. and Willems, P.J. (1995) CRASH syndrome: clinical spectrum of corpus callosum hypoplasia, retardation, adducted thumbs, spastic paraparesis and hydrocephalus due to mutations in one single gene, L1. *Eur. J. Hum. Genet.*, **3**, 273–284.
11. Kenwrick, S., Jouet, M. and Donnai, D. (1996) X linked hydrocephalus and MASA syndrome. *J. Med. Genet.*, **33**, 59–65.
12. Wong, E., Kenwrick, S., Willems, P.J. and Lemmon, V. (1995) Mutations in the cell adhesion molecule L1 cause mental retardation. *Trends Neurosci.*, **18**, 168–172.
13. Bickers, D.S. and Adams, R.D. (1949) Hereditary stenosis of the aqueduct of Sylvius as a cause of congenital hydrocephalus. *Brain*, **72**, 246–262.
14. Rosenthal, A., Jouet, M. and Kenwrick, S. (1992) Aberrant splicing of neural cell adhesion molecule L1 mRNA in a family with X-linked hydrocephalus. *Nature Genet.*, **2**, 107–112.
15. Van Camp, G., Vits, L., Coucke, P., Lyonnet, S., Schrander-Stumpel, C., Darby, J., Holden, J.J.A., Munnich, A. and Willems, P.J. (1993) A duplication in the L1CAM gene associated with X-linked hydrocephalus. *Nature Genet.*, **4**, 421–425.
16. Vits, L., Van Camp, G., Coucke, P., Fransen, E., De Boulle, K., Reyniers, E., Korn, B., Poustka, A., Wilson, G.N., Schrander-Stumpel, C., Winter, R.M., Schwartz, C.E. and Willems, P.J. (1994) MASA syndrome is due to mutations in the L1CAM gene. *Nature Genet.*, **7**, 408–413.
17. Jouet, M., Rosenthal, A., Armstrong, G., MacFarlane, J.R., Stevenson, R., Paterson, J., Matzenberg, A., Ionanescu, V., Temple, K. and Kenwrick, S. (1994) X-linked spastic paraplegia (SPG1), MASA syndrome and X-linked hydrocephalus result from mutations in the L1 gene. *Nature Genet.*, **7**, 402–407.
18. Vits, L., Chitayat, D., Van Camp, G., Holden, J.J.A., Fransen, E. and Willems, P.J. (1998) Somatic and germline mosaicism for an L1 mutation causing agenesis of the corpus callosum. *Hum. Mutat.*, Suppl. 1, S284–S287
19. Van Camp, G., Fransen, E., Vits, L., Raes, G. and Willems, P.J. (1996) A locus-specific mutation database for the neural cell adhesion molecule L1. *Hum. Mutat.*, **8**, 391.
20. Dahme, M., Bartsch, U., Martini, R., Anliker, B., Schachner, M. and Mantei, N. (1997) Disruption of the gene coding for the cell adhesion molecule L1 leads to malformations of the nervous system in mice. *Nature Genet.*, **17**, 346–349.
21. Cohen, N.R., Taylor, J.S.H., Scott, L.B., Guillery, R.W., Soriano, P. and Furley, A.J. (1997) Errors in corticospinal axon guidance in mice lacking the neural cell adhesion molecule L1. *Curr. Biol.*, **8**, 26–33.
22. Doherty, P., Williams, E.J. and Walsh, F.S. (1995) A soluble chimeric form of L1 glycoprotein stimulates neurite outgrowth. *Neuron*, **14**, 57–66.
23. Lemmon, V., Farr, K.L. and Lagenaur, C. (1989) L1-mediated axon outgrowth occurs via a homophilic binding mechanism. *Neuron*, **2**, 1597–1603.
24. Sijbers, J., Scheunders, P., Verhoye, M., Van der Linden, A., Van Dyck, D. and Raman, E. (1997) Watershed-based segmentation of 3D MR data for volume quantitation. *MRI*, **15**, 679–688.
25. Edwards, J.H., Norman, R.M. and Roberts, J.M. (1961) Sex-linked hydrocephalus: report of a family with 15 affected members. *Arch. Dis. Child.*, **36**, 481–485.
26. Macias, V.R., Day, D.W., King, T.E. and Wilson, G.N. (1992) Clasped-thumb mental retardation (MASA) syndrome: confirmation of linkage to Xq28. *J. Med. Genet.*, **43**, 408–414.

27. Boyd, E., Schwartz, C.E., Schroer, R.J., May, M.M., Shapiro, S.D., Arena, F., Lubs, H.A. and Stevenson, R.E. (1993) Agenesis of the corpus callosum associated with MASA syndrome. *Clin. Dysmorphol*., **2**, 332–341.
28. Lagenaur, C. and Lemmon, V. (1987) An L1-like molecule, the 8D9 antigen, is a potent substrate for neurite extension. *Proc. Natl Acad. Sci. USA*, **84**, 7753–7757.
29. Franklin, K.B.J. and Paxinos, G. (1997) *The Mouse Brain in Stereotactic Coordinates*. Academic Press, San Diego, CA.
30. Grant, S.G.N., O'Dell, T.J., Karl, K.A., Stein, P.L., Soriano, P. and Kandel, E.R. (1992) Impaired long-term potentiation, spatial learning, and hippocampal development in *fyn* mutant mice. *Science*, **258**, 1903–1910.
31. Wilson, M.A. and Tonegawa, S. (1997) Synaptic plasticity, place cells and spatial memory: study with second generation knockouts. *Trends Neurosci*., **200**, 102–106.
32. Bracke-Tolmitt, R., Linden, A., Canavan, A.G.M., Rockstroh, R., Scholz, E., Wessel, K. and Diener, H. (1989) The cerebellum contributes to mental skills. *Behav. Neurosci*., **103**, 442–446.
33. Lalonde, R. and Botez, M. (1990) The cerebellum and learning processes in animals. *Brain Res. Rev.*, **15**, 325–332.
34. Daum, I., Ackermann, H., Schugens, M., Reimold, C., Dichgans, J. and Birbmauer, N. (1993) The cerebellum and cognitive function in humans. *Behav. Neurosci*., **107**, 411–419.
35. Leiner, H.C., Leiner, A.L. and Dow, R.S. (1993) Cognitive and language functions of the human cerebellum. *Trends Neurosci*., **16**, 444–447.
36. Petrosini, L., Molinari, M. and Delrieu, O. (1996) Cerebellar contribution to spatial processing: Morris water maze and T-maze. *Eur. J. Neurosci*., **8**, 1882–1896.
37. Godschalk, M., van de Burg, J., van Duin, B. and De Zeeuw, C.I. (1994) Topography of saccadic eye movements evoked by microstimulation in rabbit cerebellar vermis. *J. Physiol*., **480**, 147–153.
38. Bakker, C.E., Verhey, C., Oostra, B.A., van der Helm, R., Oerlemans, F., Vermey, M., Bygrave, A., Hoogeveen, A.T., Reyniers, E., De Boulle, K., D'Hooge, R., Cras, P., van Velzen, D., Nagels, G., Martin, J.-J., De Deyn, P.P., Darby, J. and Willems, P.J. (1994) Fmr1 knock-out mice: a model to study Fragile X mental retardation. *Cell*, **78**, 23–33.
39. Yuan, C., Schmiedl, U.P., Weinberger, E., Krueck, W.R. and Rand, S.D. (1993) Three-dimensional fast spin echo imaging: pulse sequence and *in-vivo* image evaluation. *J. MRI*, **3**, 894–899.
40. De Zeeuw, C.I., van Alphen, A.M., Hawkins, R. and Ruigrok, T.J.H. (1997) Climbing fiber collaterals contact neurons in the cerebellar nuclei that provide a GABAergic feedback to the inferior olive. *Neuroscience*, **80**, 981–986.